# Characterizing the monomer-dimer equilibrium of UbcH8/Ube2L6: A combined SAXS and NMR study

*Kerem Kahraman[1], Scott A. Robson[2], Oktay Göcenler[1], Cansu D. Tozkoparan[1], Jennifer M. Klein[3], Cansu M. Yenici[1], Arthur L. Haas[3], Joshua J. Ziarek[2,]*, Çağdaş Dağ[1,4,]**

[1]Nanofabrication and Nanocharacterization Center for Scientific and Technological Advanced Research (n[2]STAR), Koc University, İstanbul, Turkey

[2]Department of Molecular and Cellular Biochemistry, Indiana University, 212 S. Hawthorne Drive, Bloomington, IN 47405, USA

[3]Department of Biochemistry and Molecular Biology, LSUHSC-School of Medicine, 1901 Perdido Street, New Orleans, LA, 70112, USA

[4]Koc University Isbank Center for Infectious Diseases (KUISCID), Koc University, Istanbul, Turkey

*Corresponding author: cdag@ku.edu.tr, jjziarek@indiana.edu

KEYWORDS. ISGylation, ubiquitination, E2 enzyme, TRACT, oligomerization

**ABSTRACT:** Interferon-stimulated gene-15 (ISG15) is an interferon-induced protein with two ubiquitin-like (Ubl) domains linked by a short peptide chain, and the conjugated protein of the ISGylation system. Similar to ubiquitin and other Ubls, ISG15 is ligated to its target proteins with a series of E1, E2, and E3 enzymes known as Uba7, Ube2L6/UbcH8, and HERC5, respectively. Ube2L6/UbcH8 plays a literal central role in ISGylation, underscoring it as an important drug target for boosting innate antiviral immunity. Depending on the type of conjugated protein and the ultimate target protein, E2 enzymes have been shown to function as monomers, dimers, or both. UbcH8 has been crystalized in both monomeric and dimeric forms, but the functional state is unclear. Here, we used a combined approach of small-angle X-ray scattering (SAXS) and nuclear magnetic resonance (NMR) spectroscopy to characterize UbcH8's oligomeric state in solution. SAXS revealed a dimeric UbcH8 structure that could be dissociated when fused with an N-terminal glutathione S-transferase molecule. NMR spectroscopy validated the presence of a concentration-dependent monomer-dimer equilibrium and suggested a backside dimerization interface. Chemical shift perturbation and peak intensity analysis further suggest dimer-induced conformational dynamics at ISG15 and E3 interfaces - providing hypotheses for the protein's functional mechanisms. Our study highlights the power of combining NMR and SAXS techniques in providing structural information about proteins in solution.

35 **INTRODUCTION**

36 Interferon-Stimulated Gene 15 (ISG15), also known as hUCRP or IP17, is a 15 kDa ubiquitin-like,
37 type I interferon (IFN) inducible protein [1]. ISGylation is an ubiquitin-like (Ubl) post-
38 translational modification (PTM) that involves the covalent attachment of ISG15 to target proteins
39 [2]. Similar to other Ubls, ISGylation plays important roles in various cellular processes such as
40 innate antiviral immunity, protein degradation, and signal transduction [3]. Free, unconjugated,
41 ISG15 also serves immunoregulatory functions as a cytoplasmic and secreted signaling protein in
42 eukaryotic organisms [4]. Inherited ISG15 deficiency dramatically reduces the innate immune
43 system's ability to fight viruses in mice yet only appears to cause immunoregulatory issues against
44 mycobacterial, not viral diseases, in humans [3]. Thus, the role of ISG15 in human viral
45 pathogenesis is not clearly understood.

46 The ISGylation cascade requires the sequential action of three enzymes: Ube1L as the E1 enzyme,
47 UbcH8 as the E2 enzyme, and HERC5 as the E3 enzyme. First, ISG15 binds the catalytically active
48 cysteine of the Ube1L activating enzyme (E1) in an ATP-dependent reaction. Then, E1 interacts
49 with UbcH8 conjugating enzyme (E2) through its ubiquitin folding domain (UFD), which
50 facilitates the transesterification of active ISG15, and results in an intermediate ISG15-UbcH8
51 complex joined by a thioester bond [5]. Finally, HERC5 ligase enzyme (E3) interacts with the
52 intermediate ISG15-UbcH8 complex to mediate ligation of ISG15 to the target protein. UbcH8
53 plays a central role in ISGylation as it interacts with both E1 and E3 enzymes - making it a key
54 target for the regulation of the ISGylation pathway [6].

55 Under reducing conditions, E2 enzymes can spontaneously form dimers when a crosslinker is
56 added [7], and apart from a few exceptions, E2 enzymes are capable of preserving their dimer form

57 [8, 9]. Nevertheless, both the dimer and the monomer forms of E2 enzymes are capable of
58 recruiting E3 enzymes and conjugating ubiquitin [10]. Although dimeric E2 enzymes are perceived
59 as more advantageous because one of the monomers can remain associated while the ubiquitin
60 conjugation continues with the other.

61 The Protein DataBank (PDB) contains both dimeric (PDB ID:1WZV) and monomeric (PDB
62 ID:1WZW) crystal structures of UbcH8. Yet, it is unknown whether UbcH8 dimerizes naturally
63 or as a consequence of non-specific crystal packing contacts. In this study, we aimed to
64 characterize the oligomeric state of human UbcH8 (Ube2L6) in solution using Small Angle X-ray
65 Scattering (SAXS). We first used a fusion protein approach with the goal of producing a high-
66 resolution scattering envelope to properly place the UbcH8 protomers. Surprisingly, UbcH8
67 formed stable dimers upon removal of the N-terminal fusion protein. We next used solution nuclear
68 magnetic resonance (NMR) spectroscopy to first validate and then further characterize the
69 monomer-dimer equilibrium. Our results indicate that UbcH8 contains a substantial dimer
70 population at 150 μM concentration and that dimerization may induce conformational changes at
71 the distal ISG and E3 interaction interfaces.

72 **RESULTS**

73 **GST fusion guides SAXS protein structural modeling.** To determine the state of UbcH8 in
74 solution, we expressed and purified it fused to an N-terminal glutathione-S transferase (GST) tag
75 herein termed GST-UbcH8. We hypothesized that the 28 kDa GST molecule should be easily
76 discernible from the smaller (18 kDa) UbcH8, and would dramatically improve fitting SAXS
77 scattering data to the structural model. The sample was concentrated to 280 μM and six, 10 min
78 SAXS frames were collected for a total of one hour. Superimposition of each 10 min frame

79 confirmed that the X-ray beam produced little to no detectable radiation damage (data not shown).
80 The medium to high q region, which is emphasized in the q vs l(q) plot, is consistent with a folded
81 sample (Figure 1A). The Kratky plot possessed a bell-shaped curve that approaches zero after
82 reaching a maximum at ~3 sRg; this result is consistent with a properly folded, globular protein
83 (Figure 1B). While slight deviations between the typical Kratky plot and dimensionless Kratky
84 plot can aid in the assessments of flexibility, no apparent differences were observed.

85 The pair-distance distribution function, P(r), is a measure of the frequency of interatomic
86 distances that can also provide information about the protein shape. The presence of a shoulder in
87 the P(r) suggests a multidomain protein as expected for the GST-UbcH8 fusion (Figure 1C). The
88 largest distance ($D_{max}$) in the P(r) histogram was 8 nm (Figure 1C). The GST-UbcH8 crystal
89 structures were then fitted into the final 3D DAMMIF dummy atom model (Figure 1D,E). Both
90 GST and UbcH8 proteins, as well as the linker peptide, are clearly visible fitting a monomeric
91 model. The fact that even the linker region can be detected with SAXS analysis and be observed
92 this clearly, underscores the power of SAXS in structure determination. After GST cleavage,
93 UbcH8 was observed to form a dimer based on Size Exclusion Chromatography (data not shown),
94 hence we hypothesized that GST mayblock the dimerization site.

95 **FreeUbcH8 is a Dimer in Solution.** To test how well the GST-fusion improves the modeling
96 of UbcH8 into the SAXS scattering, we prepared a second UbcH8 sample with the GST protein
97 removed. Again, we concentrated UbcH8 to 280 μM and collected six, 10 min frames for a total
98 of 1 h (Figure 2A). Similar to GST-UbcH8, the Kratky plot possessed a bell-shaped curve that
99 approaches zero (Figure 2B). We estimated a slightly larger $R_g$ ~ 4.40 nm, compared to GST-
100 UbcH8, from the low q region, whereas the P(r) $D_{max}$ was reduced to 6.2 nm (Figure 2C).
101 Surprisingly, the free UbcH8 P(r) also contained a shoulder suggesting homodimerization (Figure

102 2C). ATSAS molecular weight analysis predicts a 39.5 kDa particle, which is approximately
103 double the expected 18 kDa UbcH8. We then fitted the UbcH8 dimer crystal structure (PDB
104 1WZV; Figure 2D) to the dummy atom model the scattering envelope (Figure 2E). The best-fit
105 model ($X^2$ = 1.7) possesses a dimerization interface with the active site cysteines of each protomer
106 pointed outwards (Figure 2D,E). The consistency between the previously published dimer crystal
107 structure and the dummy atom model obtained by SAXS analysis, supports the homodimer
108 formation of UbcH8 protein in solution in absence of a GST-tag.

109 **NMR analysis of UbcH8 monomer-dimer equilibrium.** To further establish dimerization of
110 UbcH8 in solution, we performed Transverse Relaxation Optimized Spectroscopy (TROSY) for
111 rotational correlation times (TRACT) experiments [11,12] to estimate the rotational correlation
112 time ($\tau_c$) of UbcH8 at two different concentrations: 300 μM and 150 μM (Figure 3). The signal
113 intensity ranging from 8.6 to 9.2 ppm was integrated to maximize signal to noise and emphasize
114 well-structured regions of the protein that are representative of global tumbling. We estimated $^{15}$N
115 relaxation rates for the TROSY and anti-TROSY integrated signals using Bayesian Parameter
116 Estimation of a two-parameter single-exponential decay model. This method produces a
117 distribution of decay rates, which encompass uncertainty, that were then used to determine the
118 cross-correlated relaxation (CCR) rate. The rotational correlation time was estimated from CCR
119 according to an algebraic solution [12] of the modified Goldman relation [13], assuming an order
120 parameter ($O^2$) of 0.8. We determined a $\tau_c$ ~16 ns at 300 μM and ~13 ns at 150 μM (Figure 3),
121 which demonstrates a concentration dependence on molecular rotation diffusion times. We then
122 used hydroNMR [14] to model rotational diffusion of monomeric and dimeric UbcH8 from the
123 PDB 1WZV dimeric crystal structure. hydroNMR reported a $\tau_c$ = 20.5 ns for the dimer and 7.4 ns
124 for the monomer at 25 ºC. Taken together, this confirms that UbcH8 undergoes monomer-dimer

125 exchange and indicates a substantial dimer population even at 150 μM. Data could not be collected
126 at lower concentrations due to the sensitivity limit of the room temperature NMR probe.

127 We next collected $^{15}N$ heteronuclear single quantum coherence (HSQC) solution NMR spectra
128 at 150 μM and 300 μM to identify UbcH8's dimerization interface. Resonances were assigned by
129 visual inspection using BMRB Entry ID 16321 as a reference list. The NH resonances of all
130 residues except for the 18 prolines were assigned (79.85% completion). We then assessed both
131 concentration-dependent chemical shift perturbations (CSPs) and peak intensity differences. The
132 concentration-dependent CSPs were of relatively low magnitude and located far from the
133 crystallographic dimerization interface (Figure 4). All of the perturbed residues except for N23,
134 which resides at the dimerization site, are situated at either the E1 or the ISG15 interaction surfaces.
135 Residues E80, N81, and G82 are clustered on a loop near the catalytic C85 residue where ISG15
136 is covalently attached. Whereas F56, K99, V103, L104, and N108 are proximal to the E1 binding
137 region on the UbcH8 surface; interestingly, these residues are arranged towards the UbcH8 core
138 rather than at the surface (Figure 4). Given that ISG15 and E1 involve distinct interfaces, we
139 hypothesize a conformational change or allosteric pathway influences the transfer or binding of
140 ISG15. Our results suggest that dimerization may play an additional role in ISGylation. We
141 hypothesize that the weak CSPs could reflect a mostly sidechain-mediated interface and/or that the
142 ensemble is predominantly dimeric even at 150 μM concentration.

143 Thus, we also measured the concentration-dependent changes in peak intensity. We hypothesize
144 these intensity differences result from monomer-dimer exchange on the intermediate
145 (microsecond-millisecond) timescale, but it's also possible that they reflect dimerization-
146 dependent fluctuations in longitudinal ($T_1$) or transverse ($T_2$) relaxation. The largest changes in
147 peak intensity again clustered to the ISG15 and E1 interfaces, while also highlighting an extended

148 region along the crystalized dimer interface (Figure 5). D149 sits at the center of the dimerization
149 surface with E141 and L144 in close proximity. It's plausible that D28 and A29, located in a loop
150 region of the opposing protomer, could possess the flexibility to interact. Furthermore as the
151 overall structure gets bigger with the dimerization, decreased signals from some peaks were
152 expected due to line broadening. Although unlike the CSP analysis which showed that most of the
153 conformational changes occurred away from the dimerization site, delta chemical shift intensity
154 analysis revealed that most of the affected residues were on the dimerization site. In fact, the peak
155 intensity of N23 and D149 residues (Supp. Figure 4) from opposing protomers, which are within
156 3.3 Å distance in the crystal structure, deviated from the mean peak height by 44.7% and 62.2%,
157 at 150μM, and 37.6% and 35.6%, at 300 μM, respectively. Taken together, this indicates that
158 dimerization is *ipso facto* involved in defining interaction dynamics between E1 and E2 enzymes.

159 **DISCUSSION**

160 In this study, we investigated the oligomeric state of UbcH8 in solution using Small Angle X-ray
161 Scattering (SAXS) and NMR analysis. To improve the fitting of SAXS scattering data to the
162 structural model, we initially employed an N-terminal GST-fused UbcH8 protein. The results from
163 SAXS experiments and analysis indicate that the GST-UbcH8 fusion protein is monodisperse and
164 properly folded in solution. The 3D DAMMIF dummy atom model also revealed a monomeric
165 model of the GST-UbcH8 fusion protein, highlighting the advantages of SAXS in structure
166 determination. The free form of UbcH8, without the GST fusion, was further investigated.
167 Surprisingly, the P(r) distribution suggested a multidomain complex, and the ATSAS molecular
168 weight analysis indicated dimer formation. The consistency between the existing crystal structure
169 of UbcH8 dimer and the SAXS-derived dummy atom model supports the formation of a UbcH8
170 homodimer in solution in the absence of a GST-tag.

171 Our NMR analysis, including chemical shift perturbation and peak intensity measurements,
172 provide additional evidence for the dimerization of UbcH8. Residues involved in the dimerization
173 process were identified, and the effects of dimerization on the E1 and ISG15 interaction sites were
174 observed. The TRACT experiments also supported the dimerization of UbcH8, revealing a
175 concentration-dependent behavior of UbcH8 in solution, which suggests monomer-dimer
176 exchange on an intermediate timescale. The dimerization of UbcH8 and its implications on the
177 ISGylation process are consistent with previous reports of E2 enzymes forming dimers to facilitate
178 polyubiquitination [10]. Dimerization of several E2 enzymes are reported and the observed
179 dimerization of the enzymes are found to be stimulating the catalytic activity of the E2 enzyme in
180 these studies [9,15,16,17]. In 2010, David et. al. suggested that E2 enzymes form dimers in
181 solution regardless if an active ubiquitin is present [7]. While the monomer form is also active for
182 the acquisition of the ubiquitin, dimer form of the E2 is found to be more advantageous as while
183 one monomer site is binding the ubiquitin molecules, the other site is capable of remaining
184 associated to the target protein and thus facilitates efficient polyubiquitination. The acting
185 mechanism of E2 enzymes proposed in this study suggests that the E2 enzymes function as dimers
186 while catalyzing polyubiquitination process [7]. Our results demonstrate that UbcH8, the E2
187 enzyme specific for ISGylation, can also form dimers at near physiological concentrations. This
188 suggests that the ISGylation process may also involve dimerization for regulating the complicated
189 interactions of E1, E2 and E3 enzymes. This study highlights the importance of understanding the
190 oligomeric state and behavior of proteins in solution to gain insights into their biological function
191 and regulation. Moreover, our work emphasizes the usefulness of SAXS and NMR techniques in
192 elucidating protein structures and interactions in solution, which can complement crystallographic
193 studies and provide a more biologically relevant context.

194 Future studies may focus on exploring the functional implications of UbcH8 dimerization in the
195 ISGylation process, such as the effects on substrate specificity, E1 and E3 enzyme interactions,
196 and the kinetics of ISGylation. Additionally, the molecular mechanisms underlying the observed
197 concentration-dependent behavior of UbcH8 and the role of post-translational modifications in
198 modulating its oligomeric state could be investigated further. These studies will contribute to a
199 more comprehensive understanding of the regulation and function of UbcH8 in the context of
200 ISGylation and its broader implications in various diseases, including viral and bacterial infections,
201 cancer, and autoimmune disorders.

202

203 **MATERIALS AND METHODS**

204 **Protein expression and purification.** Three alanine residues followed by the coding sequence
205 of the UbcH8 protein are inserted in the 5' BamH1/ 3' EcoR1 restriction sites of the pGEX-4T3
206 plasmid. Three alanine residues are inserted between the GST and UbcH8 protein sequence in
207 order to increase the binding efficiency and also to provide a better cleavage upon thrombin
208 treatment during the purification of the protein sample. The final coded amino acid sequence
209 was:MSPILGYWKIKGLVQPTRLLLEYLEEKYEEHLYERDEGDKWRNKKFELMGLEFPNL
210 PYYIDGDVKLTQSMAIIRYIADKHNMLGGCPKERAEISMLEGAVLDIRYGVSRIAYSKDF
211 ETLKVDFLSKLPEMLKMFEDRLCHKTYLNGDHVTHPDFMLYDALDVVLYMDPMCLDA
212 FPKLVCFKKRIEAIPQIDKYLKSSKYIAWPLQGWQAFGGGDHPPKSDLVPRGSAAAMAS
213 MRVVKELEDLQKKPPPYLRNLSSDDANVLVWHALLLPDQPPYHLKAFNLRISFPPEYPF
214 KPPMIKFTTKIYHPNVDENGQICLPIISSENWKPCTKTCQVLEALNVLVNRPNIREPLRMD
215 LADLLTQNPELFRKNAEEFTLRFGVDRPS*

216 pGEX-4T3 GST-AAA-UbcH8 plasmid was transformed into Rosetta2 *E. Coli* expression cells,
217 plated on LB-ampicillin-chloramphenicol, and grown overnight at 37 °C. The next morning,
218 colonies were picked from the agar plate and inoculated into 10 ml LB-ampicillin-chloramphenicol
219 medium. The culture was grown overnight at 37 °C at 110 rpm. The overnight culture was
220 transferred into 1 L LB medium and incubated at 37°C. After $OD_{595}$ exceeded 0.3, temperature
221 was lowered to 18°C and protein production was induced at $OD_{595}$ 0.8 by the addition of 0.4mM
222 IPTG. Cells were harvested 18 hours after induction by centrifugation at 2000 RCF for 1 hour.

223 Harvested cells were resuspended in lysis buffer (500mM NaCl, 50mM Tris, 0.1% (v/v) Triton X-
224 100, 5% (v/v) glycerol, 1mM DTT, pH=7.5), sonicated, and centrifuged at 20K RCF for 1 hour to
225 remove insoluble debris. The obtained supernatant was loaded to a GST affinity column
226 equilibrated with 20mM Tris (pH 7.5), 150mM NaCl, 1mM DTT. Non-specific proteins were
227 washed with the same buffer and the protein was eluted with 30mM glutathione, 20mM Tris (pH
228 7.5), 150mM NaCl, 1mM DTT. For cleavage of the GST tag, 1:100 thrombin enzyme was added
229 to the eluted protein and dialyzed in 20mM Tris (pH 7.5), 150mM NaCl, 1mM DTT solution
230 overnight to eliminate excess glutathione. For separation of the GST tag, reverse GST
231 chromatography was applied. Unbound free UbcH8 was collected and purified by size exclusion
232 chromatography using 20mM Tris (pH 7.5), 150mM NaCl, 1mM DTT buffer.

233

234 **SAXS Data Collection.** All SAXS data were collected at home source SAXSpoint 5.0 (Anton
235 Paar GmbH) as described before [18]. Sample/detector distance (SDD) was 1600 mm for SAXS
236 experiments. All measurements took place at 10 °C. Data was collected in one hour session(1-
237 minutes long 6 frames) for each measurement. The scattering curves were checked for radiation

238 damage and no damage was detected after the superimposition of each 10 minute data collection
239 intervals..

240 **SAXS Data Processing and Modeling.** At first, the scattering pattern of all samples were
241 visually inspected in the Primus program of ATSAS 3.0 for any possible issues with the
242 measurement[11]. The radius of gyration (Rg) was calculated using Guinier's equation and inverse
243 Fourier transform by Primus. Distance distribution function P(r) and the maximum particle
244 diameter (Dmax) was calculated by GNOM[19]. After estimating the molecular weight of the
245 model DAMMIF (ab initio) is used to generate 5 independent low resolution models from the data.
246 [20]. DAMAVER and DAMMIN then averaged, clustered, and optimized these 5 distinct solutions
247 to form the final ab-initio shape [21]. SASpy plug-in for PyMOL was used to superimpose the
248 homology modeled structure of the protein [22, 23].

249 **$^{15}$N Labeled Protein Expression and Purification.** pGEX-4T3 GST-AAA-UbcH8 plasmid
250 containing bacteria were grown overnight in LB medium at 37°C and transferred into 50 mL $^{15}$N
251 labeled M9 media the next day. Following 4 hours of incubation at 37°C, cells were transferred
252 into 1L M9 media. After $OD_{595}$ exceeded 0.3, temperature was lowered to 18°C and protein
253 production was induced at $OD_{595}$ 0.8 by the addition of 0.4mM IPTG. The medium contained
254 33.7mM $Na_2HPO_4$, 22 mM $KH_2PO_4$, 8.55 mM NaCl, 9.35 mM $^{15}$N labeled $NH_4Cl$, 1mM $MgCl_2$,
255 0.3mM $CaCl_2$, and 7 mg/L $FeCl_2$-$4H_2O$. Cells were harvested 18 hours after induction by
256 centrifugation at 2000 RCF for 1 hour.

257 Harvested cells were resuspended in lysis buffer (500mM NaCl, 50mM Tris, 0.1% (v/v) Triton X-
258 100, 5% (v/v) glycerol, 1mM DTT, pH=7.5), sonicated, and centrifuged at 20K RCF for 1 hour to
259 remove insoluble debris. The obtained supernatant was loaded to a GST affinity column

260 equilibrated with 38.39 mM $Na_2HPO_4$, 11.61 mM $KH_2PO_4$ (pH 7.4), 100 mM NaCl, 1mM DTT.
261 Non-specific proteins were washed with the same buffer and the protein was eluted with 30mM
262 glutathione, 38.39 mM $Na_2HPO_4$, 11.61 mM $KH_2PO_4$ (pH 7.4), 100 mM NaCl, 1mM DTT. For
263 cleavage of the GST tag, 1:100 thrombin enzyme was added to the eluted protein and dialyzed in
264 38.39 mM $Na_2HPO_4$, 11.61 mM $KH_2PO_4$ (pH 7.4), 100 mM NaCl, 1mM DTT solution overnight
265 to eliminate excess glutathione. For separation of the GST tag, reverse GST chromatography was
266 applied. Unbound free UbcH8 was collected and purified by size exclusion chromatography using
267 38.39 mM $Na_2HPO_4$, 11.61 mM $KH_2PO_4$ (pH 7.4), 100 mM NaCl, 1mM DTT buffer.

268

269 **NMR Data Acquisition and analysis.** The protein was concentrated to 0.287 mM. 10% D2O
270 (final concentration) containing 1mM DSS was added to obtain a final sample volume of 600 µL.
271 All NMR data acquisition process was completed using 500 MHz Bruker Ascend magnet equipped
272 with Avance NEO console and BBO double resonance room temperature probe at Koç University
273 $n^2$STAR NMR Facility. 2-D $^1$H-$^{15}$N HSQC spectra were recorded with 50% non-uniform sampling
274 (NUS) at 298 K with a 1H spectral width of 14 ppm (1024 data points in t2) and a $^{15}$N spectral
275 width of 32 ppm (64 data points in t1). The 2D data was processed by NMRPipe [24] and analyzed
276 using NMRFAM-SPARKY [25]. The combined $^1$H-$^{15}$N chemical shift perturbations were
277 calculated using equation $\Delta\delta_{AV} = [(\Delta\delta\ ^1H)^2 + (\Delta\delta\ ^{15}N*0.14)^2]^{1/2}$ [26].

278 1D TRACT experiments [11] were collected with 1024 complex points and 1.5 s recycle delay.
279 Relaxation rates for $^{15}$N TROSY and anti-TROSY components were determined from spectra
280 intensity values integrated over 9.2 to 8.6 ppm at eight relaxation delays: 30, 60, 90, 120, 150, 180,
281 210, 240, 270 and 300 ms. Each relaxation rate and its uncertainty was estimated by fitting the

integrated values and time delays to a single parameter exponential decay model using Bayesian Parameter Estimation. Each TROSY and anti-TROSY relaxation rate was then used to estimate rotational correlation time ($\tau_c$) using the algebraic method [12] where we assumed an order parameter ($O^2$) of 0.8.

**Author Contributions**

**Çağdaş Dağ:** Conceptualization, Methodology, Supervision Funding acquisition, Writing-Reviewing and Editing, Writing-Original draft preparation **Joshua J. Ziarek:** Conceptualization, Writing- Reviewing and Editing, Writing- Original draft preparation **Arthur L. Haas:** Conceptualization, Supervision **Kerem Kahraman**: Investigation, Formal analysis, Visualization. **Scott A. Robson:** Investigation, Formal analysis, Visualization, Writing- Reviewing and Editing **Oktay Göcenler:** Formal analysis, Investigation Writing - Original Draft, Visualization **Cansu D. Tozkoparan:** Visualization, Formal analysis **Jennifer M. Klein:** Investigation, **Cansu M. Yenici:** Investigation

**ACKNOWLEDGMENT**

CD acknowledges support from TÜBİTAK (Project No: 120Z594, 122Z747). JJZ acknowledges support from National Institutes of Health grant R35GM143054. The authors acknowledge the use of the services and facilities of n$^2$STAR-Koç University Nanofabrication and Nanocharacterization Center for Scientific and Technological Advanced Research.

301 **REFERENCES**

302 [1] Haas, A. L., Ahrens, P., Bright, P. M., Ankel, H. (1987) Interferon induces a 15-kilodalton
303 protein exhibiting marked homology to ubiquitin. Journal of Biological Chemistry, 262(23),
304 11315-11323.

305 [2] Loeb, K. R., Haas, A. L. (1992) The interferon-inducible 15-kDa ubiquitin homolog conjugates
306 to intracellular proteins. Journal of Biological Chemistry, 267(11), 7806-7813.

307 [3] Perng, YC., Lenschow, D.J. (2018) ISG15 in antiviral immunity and beyond. Nat Rev
308 Microbiol 16, 423–439

309 [4] Swaim CD, Scott AF, Canadeo LA, Huibregtse JM. (2017) Extracellular ISG15 Signals
310 Cytokine Secretion through the LFA-1 Integrin Receptor. Mol Cell, 68(3):581-590

311 [5] Durfee, L. A., Kelley, M. L., Huibregtse, J. M. (2008) The basis for selective E1-E2
312 interactions in the ISG15 conjugation system. Journal of Biological Chemistry, 283(35), 23895-
313 23902.

314 [6] Stewart, M. D., Ritterhoff, T., Klevit, R. E., Brzovic, P. S. (2016) E2 enzymes: more than just
315 middle men. Cell research, 26(4), 423-440.

316 [7] David, Y., Ziv, T., Admon, A., Navon, A. (2010) The E2 ubiquitin-conjugating enzymes direct
317 polyubiquitination to preferred lysines. Journal of Biological Chemistry, 285(12), 8595-8604.

318 [8] Vittal, V., Wenzel, D. M., Brzovic, P. S., Klevit, R. E. (2013). Biochemical and structural
319 characterization of the ubiquitin-conjugating enzyme UBE2W reveals the formation of a
320 noncovalent homodimer. Cell biochemistry and biophysics, 67(1), 103-110.

[9] Liess, A. K., Kucerova, A., Schweimer, K., Schlesinger, D., Dybkov, O., Urlaub, H., ... & Lorenz, S. (2020) Dimerization regulates the human APC/C-associated ubiquitin-conjugating enzyme UBE2S. Science signaling, 13(654), eaba8208.

[10] Bremm, A. (2020) Hug and hold tight: Dimerization controls the turnover of the ubiquitin-conjugating enzyme UBE2S. Science Signaling, 13(654), eabd9892.

[11] Lee, D., Hilty, C., Wider, G., Wuthrich, K. (2006) Effective rotational correlation times of proteins from NMR relaxation interference. J Magn Reson 178, 72–6.

[12] Robson, S. A., Dağ, Ç. Wu, H., Ziarek, J. J. (2021) Journal of Biomolecular NMR volume 75, 293–302.

[13] Goldman, M. (1984) Interference effects in the relaxation of a pair of unlike spin-12 nuclei. Journal of Magnetic Resonance 60, 437–452.

[14] J García de la Torre, M.L Huertas, B Carrasco (2000) HYDRONMR: Prediction of NMR Relaxation of Globular Proteins from Atomic-Level Structures and Hydrodynamic Calculations, Journal of Magnetic Resonance, 147, 1.

[15] Liu, W., Shang, Y., Zeng, Y., Liu, C., Li, Y., Zhai, L., ... Li, W. (2014) Dimeric Ube2g2 simultaneously engages donor and acceptor ubiquitins to form L ys48-linked ubiquitin chains. The EMBO journal, 33(1), 46-61.

[16] Li, W., Tu, D., Brunger, A. T., Ye, Y. (2007). A ubiquitin ligase transfers preformed polyubiquitin chains from a conjugating enzyme to a substrate. Nature, 446(7133), 333-337.

[17] Varelas, X., Ptak, C., Ellison, M. J. (2003). Cdc34 self-association is facilitated by ubiquitin thiolester formation and is required for its catalytic activity. Molecular and cellular biology, 23(15), 5388-5400.

[18] Göcenler, O. , Yenici, C. M. , Kahraman, K. , Büyükdağ, C. & Dağ, Ç. (2022). Biomolecular Solution X-Ray Scattering At n2STAR Beamline. Mugla Journal of Science and Technology , 8 (2) , 60-69

[19] Svergun, D.I. (1992) Determination of the regularization parameter in indirect-transform methods using perceptual criteria. J. Appl. Crystallogr. 25, 495-503.

[20] Franke, D., Svergun, D.I. (2009) DAMMIF, a program for rapid ab-initio shape determination in small-angle scattering. J. Appl. Cryst., 42, 342-346.

[21] D. I. Svergun, D. I. (1999) Restoring low resolution structure of biological macromolecules from solution scattering using simulated annealing. Biophys J. 2879-2886.

[22] Schrödinger, L., DeLano, W. (2020) PyMOL. Retrieved from http://www.pymol.org/pymol.

[23] Panjkovich, A., Svergun, D. I. (2016) SASpy: a PyMOL plugin for manipulation and refinement of hybrid models against small angle X-ray scattering data. Bioinformatics, 32(13), 2062-2064.

[24] Delaglio, F., Grzesiek, S., Vuister, G.W. Zhu, G., Pfeifer, J., Bax, A. (1995) J. Biomol. NMR. 6, 277-293.

[25] Lee, W., Tonelli, M., Markley, J. L. (2015) NMRFAM-SPARKY: enhanced software for biomolecular NMR spectroscopy. Bioinformatics (Oxford, England), 31(8), 1325–1327.

360 [26] Williamson, M. P. (2013) Using chemical shift perturbation to characterise ligand binding,
361 Progress in Nuclear Magnetic Resonance Spectroscopy, 73, 1-16.

362

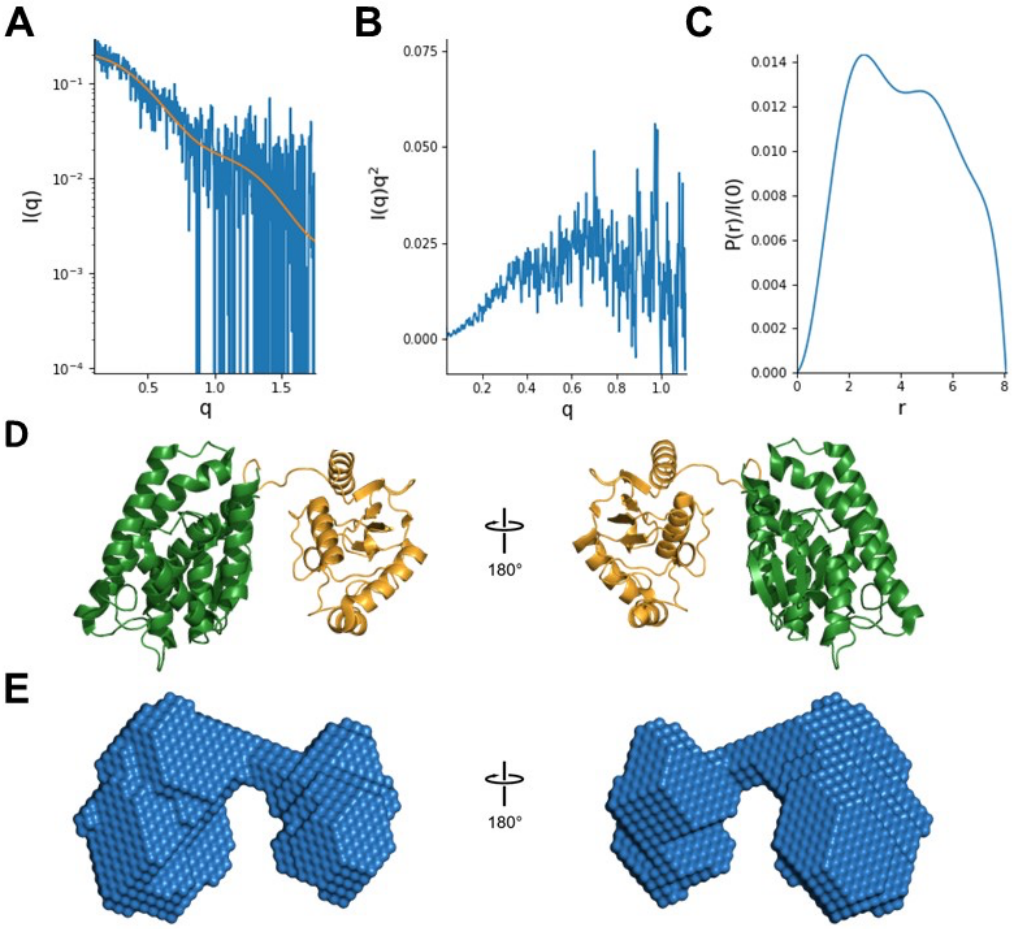


363

364 **Figure 1. SAXS analysis of GST-UbcH8 fusion protein.** (A) ln I (s) vs s plot, (B) Kratky plot,
365 and (C) Pair distance distribution, P(r), plot of the experimental SAXS intensity obtained at 4.1
366 mg/ml (280 μM) of the GST-UbcH8 fusion protein. The pair-distance distance distribution plot of
367 the GST-UbcH8 fusion protein scattering data calculated by GNOM. (D) The individual crystal
368 structures of GST (PDB:1R5A) and UbcH8 (PDB:1WZW ) shown as cartoon representations. (E)
369 The GST-UbcH8 dummy atom model, obtained by the ATSAS online package, is shown as a
370 surface representation.

371

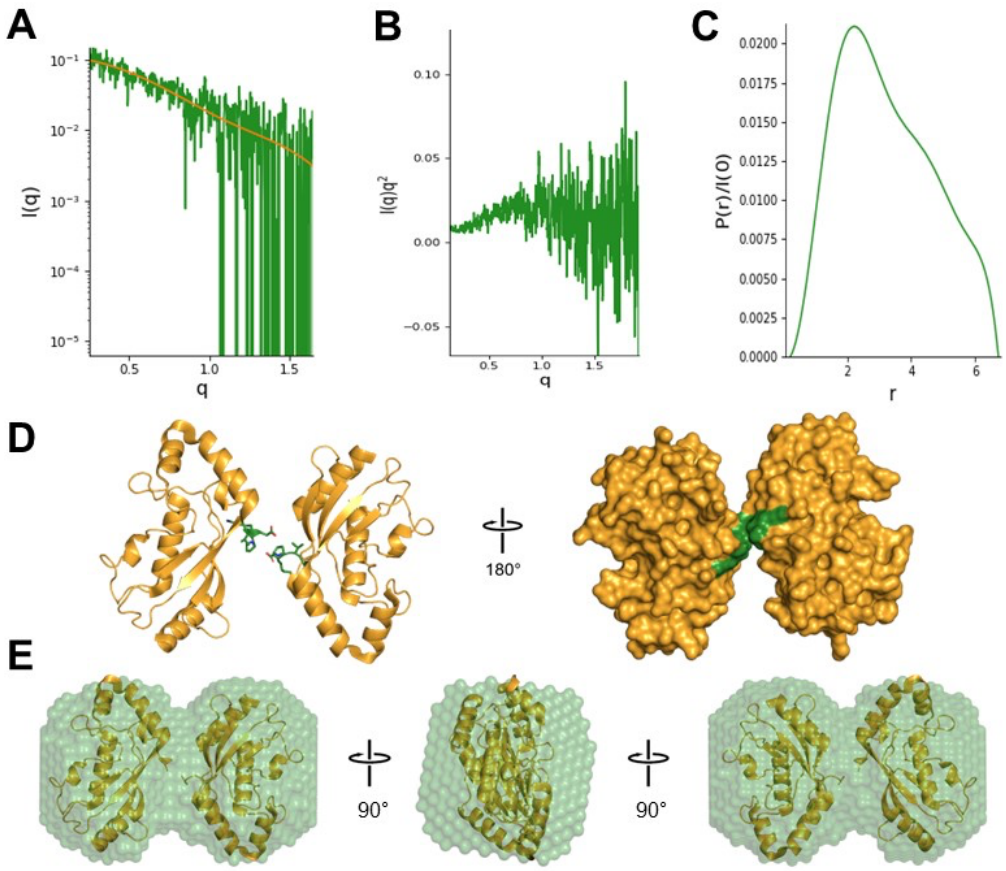


**Figure 2. SAXS analysis of free UbcH8.** (A) ln I (s) vs s plot, (B) Kratky plot, and (C) Pair distance distribution, P(r), plot of the experimental SAXS intensity obtained at 4.1 mg/ml (280 μM) free UbcH8 protein. (D) Crystal structure of UbcH8 dimer (pdb:1WZV) shown as cartoon and surface representation using Pymol. Residues D149, R150, and P151 of the dimerization interface are colored forest green. (E) UbcH8 dimer crystal structure (pdb:1WZV) fitted ($\chi = 1.02$) into the DAMMIF dummy atom model using SASpy.

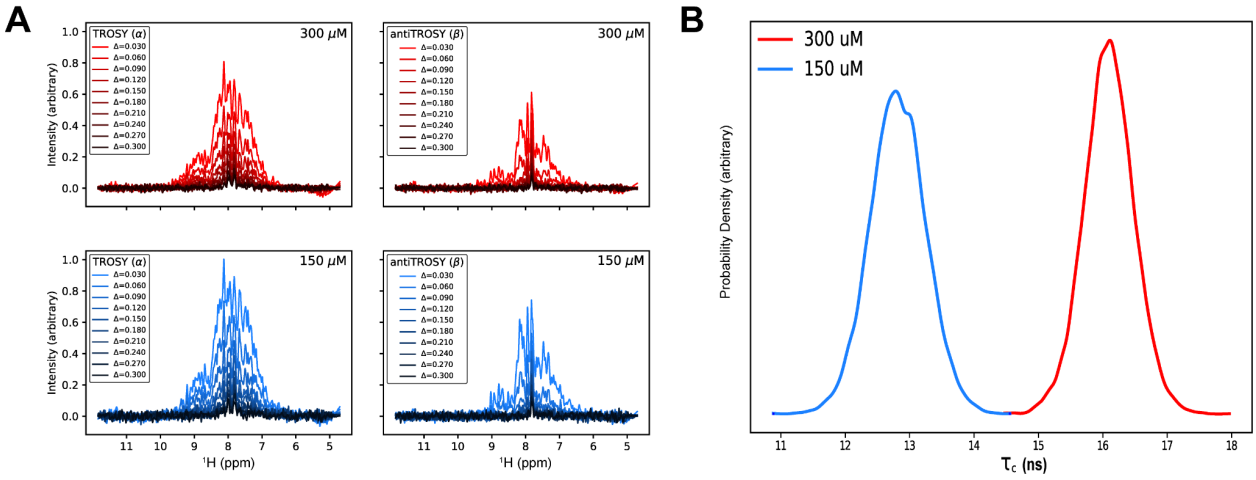


**Figure 3. TRACT analysis of free UbcH8 to determine rotational correlation time.** (A)The UbcH8 1D $^{15}$N TROSY (left) and anti-TROSY (right) spectra from the TRACT experiment. The top and bottom panels are UbcH8 at 300 (red) and 150 μM (blue), respectively. We integrate from 8.6-9.2 ppm (gray boxed region) under the assumption that it possesses resonances from primarily structured regions. (B) The probability density estimates of the overall rotational correlation time ($\tau_c$) for UbcH8 at 300 μM (red) and 150 μM (blue). The average (point) estimate for 300 μM and 150 μM UbcH8 are 16.1 ns and 12.8 ns, respectively.

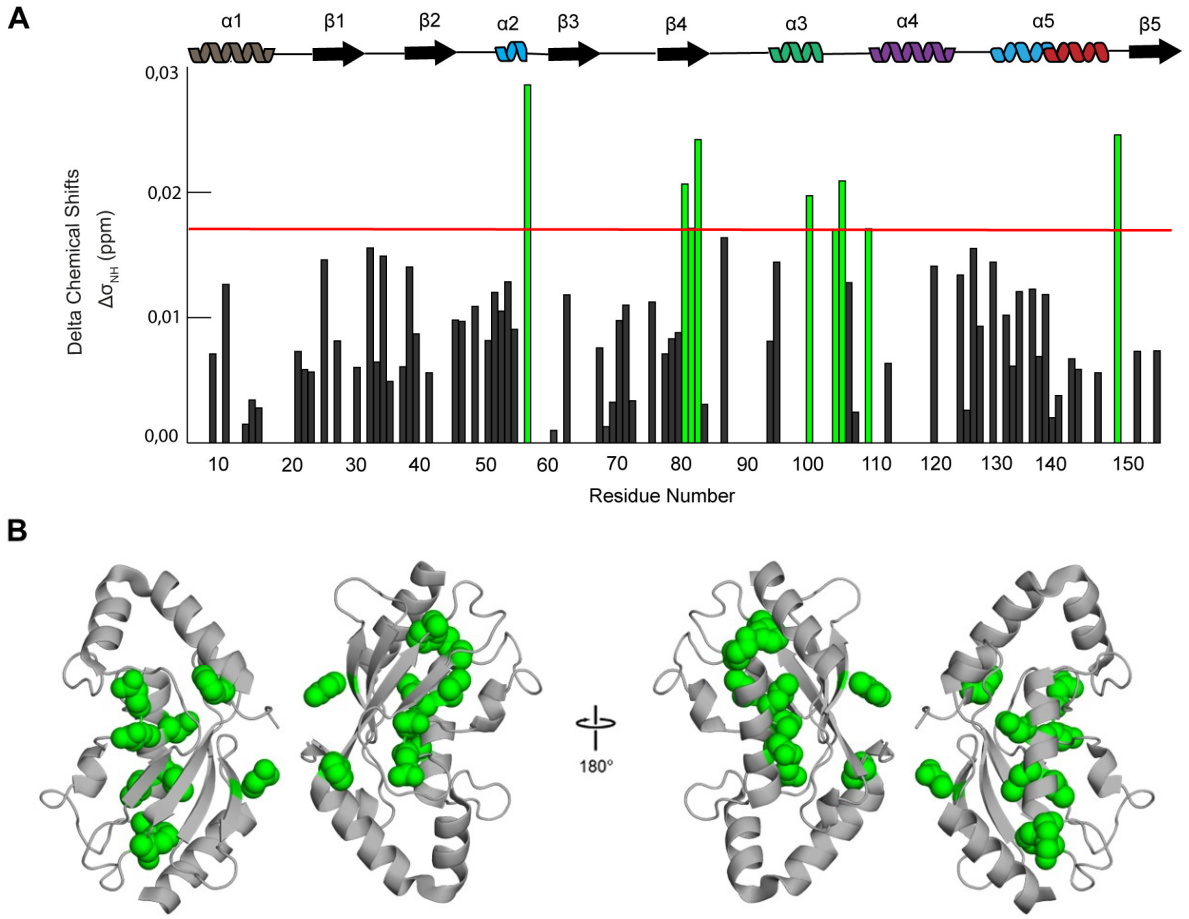


**Figure 4. $^{1}$H-$^{15}$N Chemical shift perturbations mapped onto UbcH8 dimeric crystal structure.** A) The combined $^{1}$H-$^{15}$N chemical shift perturbations between 300 μM and 150 μM UbcH8 were calculated for each residue. The residues colored green possessed chemical shift perturbations larger than the threshold (red line). Residues with no bars were not observed at either concentration. B) Residues with chemical shift perturbations larger than the threshold were mapped onto the UbcH8 dimeric crystal structure (PDB 1WZV). These residues cluster to three distinct regions: the dimer interface (N23), the ISG15 conjugation site (E80, N81, and G82), and the E1 binding surface (F56, K99, V103, L104, and N108).

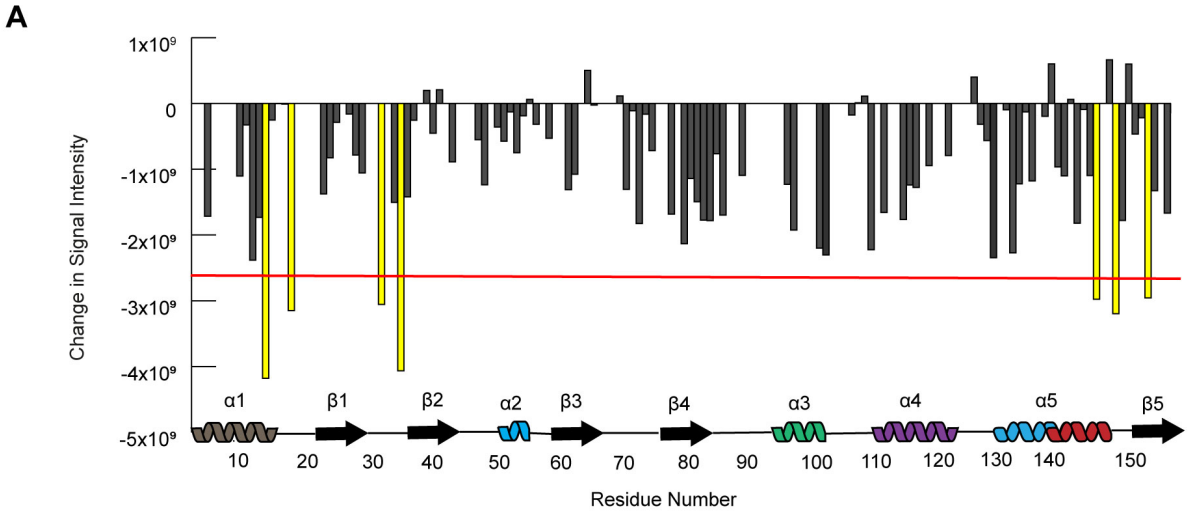


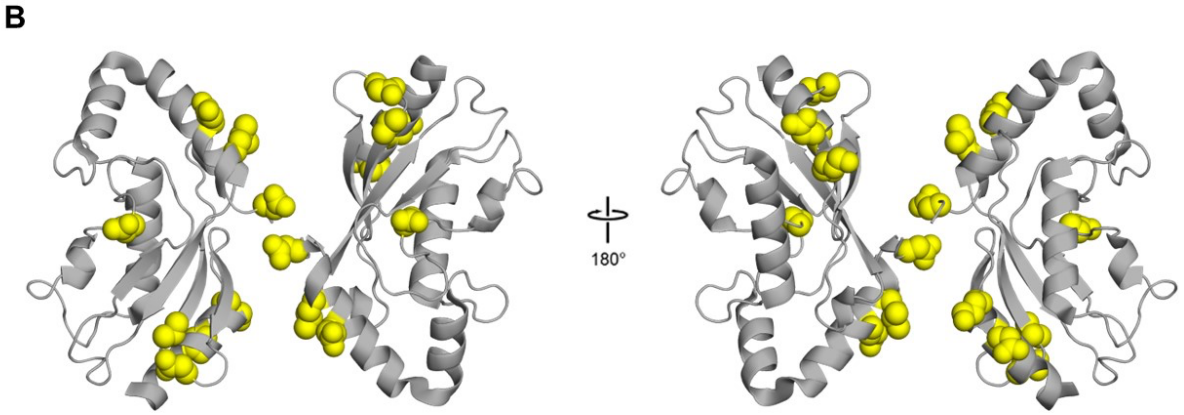


**Figure 5. Concentration dependent chemical shift signal intensity changes** A)Concentration-dependent changes in $^{1}H$-$^{15}N$ peak intensity mapped onto UbcH8 dimeric crystal structure. The residues colored yellow possessed peak intensity changes that were larger than the threshold (red line); these residues are D12, K16, N30, V33, E141, L144, and D149. Residues with no bars were not observed at either concentration. B) Residues with peak intensity changes larger than the threshold were mapped onto the UbcH8 dimeric crystal structure (PDB 1WZV).

407

408 **SUPPLEMENTARY INFORMATION**

409

410 **Supplementary Table 1.** Molecular Size Parameters of GST-UbcH8 and UbcH8 dimer Obtained

411 from SAXS Data Analysis.

| Sample | $R_g$ (nm)[a] | Dmax (nm)[b] | Vp (Å$^3$)[c] | MW (kDa)[d] | Vc (kDa)[e] | Qp (kDa)[f] |
|---|---|---|---|---|---|---|
| GST-UbcH8 | 3.37 | 8 | 8919 | 41.604 | 41.737 | 42.842 |
| UbcH8 dimer | 4.402 | 6.2 | 5835 | 39.547 | 38.766 | 44.169 |

412 [a]Radius of gyration, [b]Maximum Dimension, [c]Porod Volume, [d]Molecular Weight, [e]Volume of

413 Correlation, [f]Porod invariant

414

415 **Supplementary Table 2.** Fit quality for superimposition of E2 crystal structures onto UbcH8

416 dummy atom model. The UbcH8 dummy atom model was calculated from the SAXS data using

417 DAMMIF. The fineness and normalized spatial discrepancy (NSD) of the superimposition

418 obtained using the SASpy Pymol extension.

| | 3WE5 | 6QH3 | 6QHK | 6S98 |
|---|---|---|---|---|
| **Fineness** | 1.549 | 1.370 | 1.030 | 1.043 |
| **Normalized Spatial Discrepancy (NSD)** | 2.2294 | 3.6498 | 4.9168 | 5.3306 |

419

420

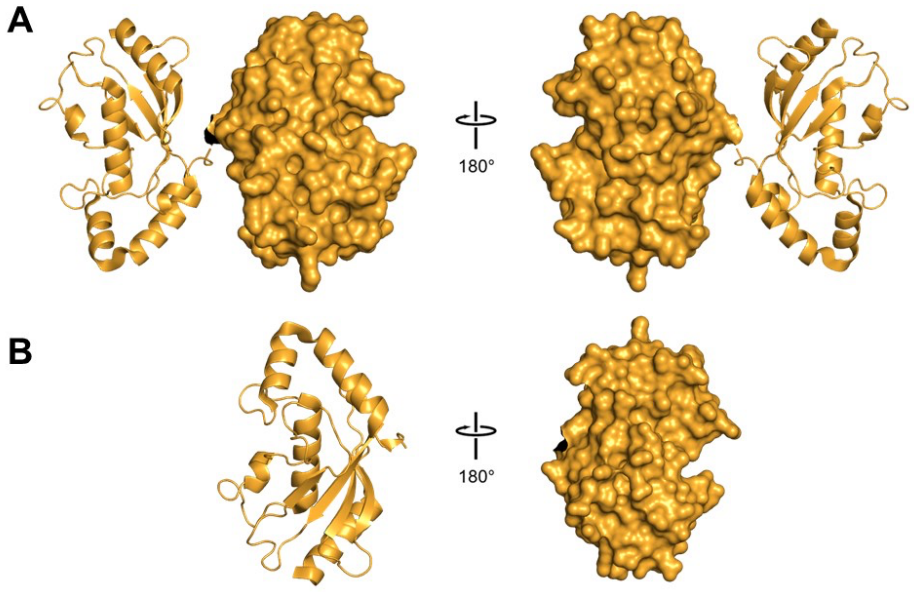


421

422 **Supplementary Figure 1. Previously-determined UbcH8 crystal structures.** Cartoon and

423 surface representation of UbcH8 protein in the (A) dimeric form (PDB ID:1WZV) and (B)

424 monomeric form (PDB ID:1WZW)

425

426

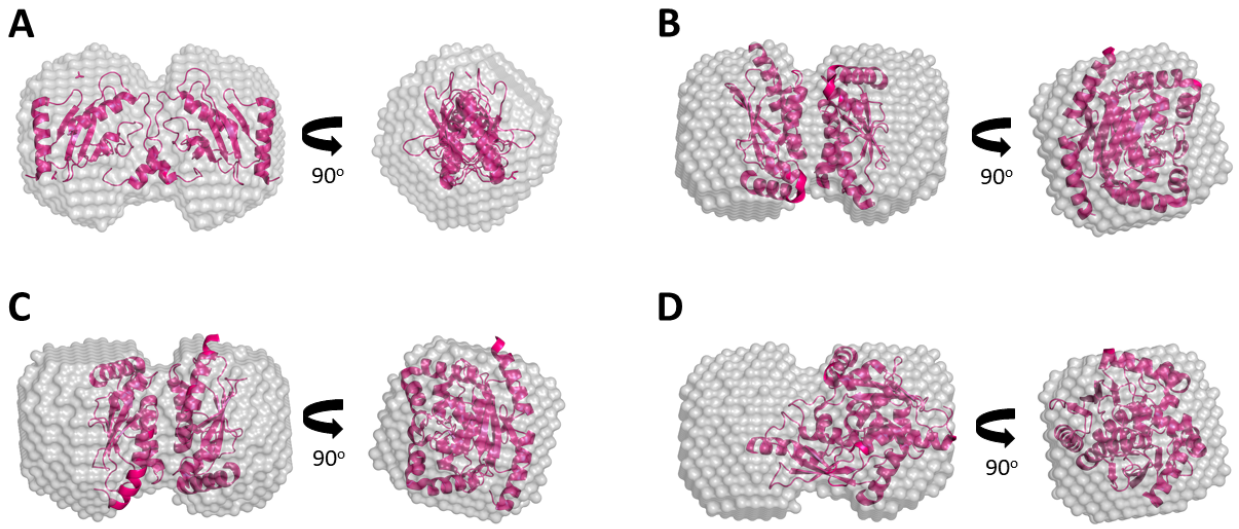


**Supplementary Figure 2. Comparison of free UbcH8 dummy atom model with previously-determined E2 enzyme crystal structures.** (A) Ubiquitin conjugating enzyme E2 UbcA1 from Agrocybe aegerita (PDB: 3WE5). (B) The catalytic domain of the human ubiquitin-conjugating enzyme UBE2S C118M (PDB: 6QH3). (C) The catalytic domain of the human ubiquitin-conjugating enzyme UBE2S (PDB: 6QHK). (D) The catalytic domain of wild-type UBE2S (PDB: 6S98). The free UbcH8 dummy atom model was calculated by DAMMIF.

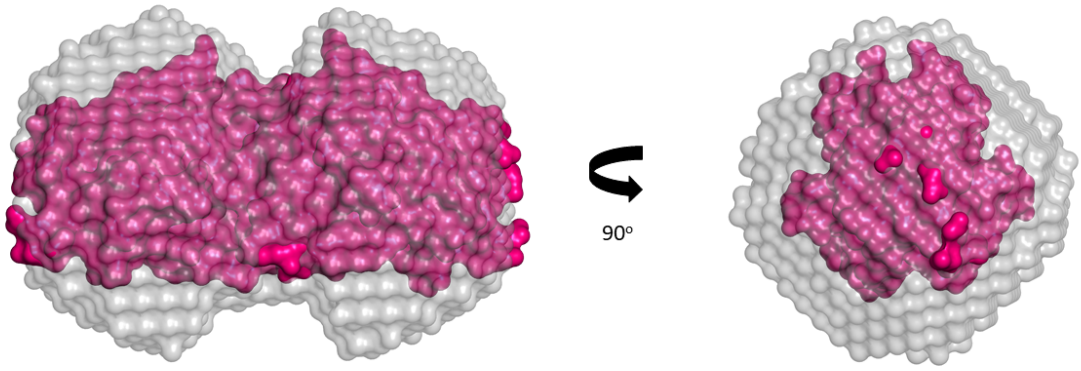


**Supplementary Figure 3. UbcA1 dimer crystal structure (pdb:1WZV) fitted into the DAMMIF dummy atom model** Crystal structure of ubiquitin conjugating enzyme E2 UbcA1 from Agrocybe aegerita (PDB: 3WE5) shown as surface (pink) placed into the dummy model of UbcH8 dimer (Free UbcH8, gray) obtained after the DAMMIF analysis of the SAXS data, using Pymol plugin SasPY.

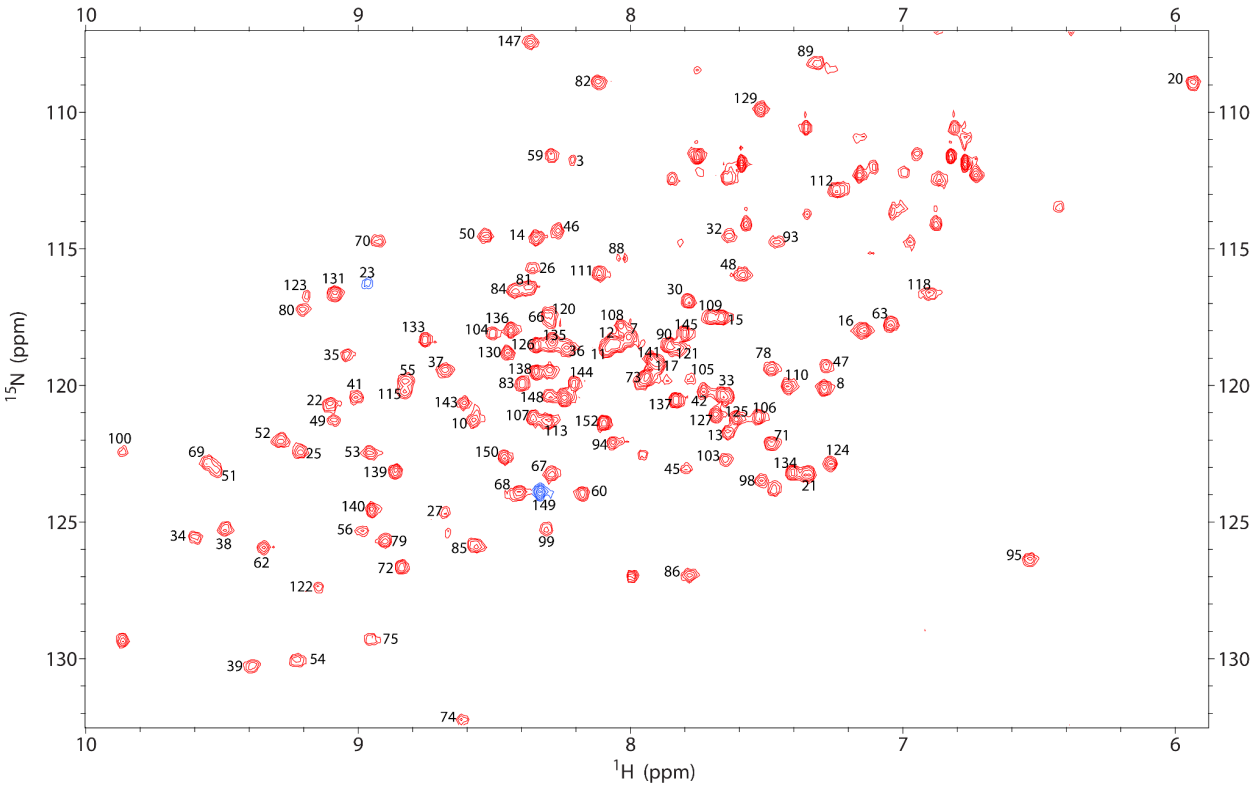


**Supplementary Figure 4. $^{1}$H-$^{15}$N HSQC spectrum of UbcH8 collected at 25°C.** Residue numbers are indicated on each peak. Resonances were assigned by visual using BMRB 16321. Data were collected at 300 µM on a 11.7 T Bruker NMR spectrometer.